# Aluminum sheet forming at elevated temperatures

A.H. van den Boogaard
*University of Twente, Department of Mechanical Engineering, Enschede, the Netherlands and Netherlands Institute for Metals Research*

P.J. Bolt & R.J. Werkhoven
*TNO Industrial Technology, Eindhoven, the Netherlands*

ABSTRACT: The formability of aluminum sheet depends on the temperature of the material and the strain rate. E.g. the limiting drawing ratio can be improved by increasing the temperature uniformly, but even more by heating the flange and cooling the punch. To accurately simulate the deep drawing or stretching of aluminum sheet at elevated temperatures, a material model is required that incorporates the temperature and strain-rate dependency. In this paper simulations are presented of the deep drawing of a cylindrical cup, using axi-symmetric elements. Two material models are compared. First a phenomenological material model is used, in which the parameters of a Ludwik–Nadai hardening curve are made temperature and strain-rate dependent. Then a physically-based model, according to Bergström is used. The model incorporates the influence of the temperature on the flow stress and on the hardening rate and includes dynamic recovery aspects.

## 1 INTRODUCTION

In deep drawing of a cylindrical cup, the limiting drawing ratio can be increased considerably by controlling the temperature of different parts of the aluminum sheet (Wilson 1988; Bolt et al. 1999; Bolt et al. 2000). By heating the flange up to 250 °C and cooling the punch the limiting drawing ratio could be increased from 2.1 to 2.6 for a 5754-O alloy in an experiment performed by the authors (see fig. 1). It

Figure 1: Limiting drawing results at 20 °C (left) and with the flange at 250 °C (right).

can be expected that the optimal temperature distribution depends on the type of aluminum and the tool geometry. In this paper experiments with the 5754-O alloy are analyzed, to determine whether a numerical analysis can predict the punch force-displacement curves and the thickness distribution of the final product. Uniaxial tensile tests were performed at 4 different temperatures and 2 strain rates. With the data from these experiments, the parameters for two material models were fitted. This is described in the next section. With these models, some deep drawing experiments were simulated. In the experiments the die and blank-holder were heated at different temperatures and the punch was kept at room temperature. The results are presented in Section 3.

## 2 MATERIAL MODEL

### 2.1 *Experiments*

Two different material models were used for the analyses. First a phenomenological model was used and secondly a so-called physically based model. The physically based model still has a number of parameters that are difficult to measure and hence are used as fitting parameters. The choice of parameters and state variables however is based on physical quantities like the dislocation densities, in contrast with the purely phenomenological models.

Both models give a flow stress as a function of the deformation path, temperature and strain rate. The translation of this (equivalent) stress to the general stress space is performed by an isotropic Von Mises yield surface.

Uniaxial tensile test experiments were performed at

temperatures of 25 °C, 100 °C, 175 °C and 250 °C at strain rates of 0.002 and 0.02 $s^{-1}$. The resulting engineering stress-strain curves are presented in Figures 2 and 3.

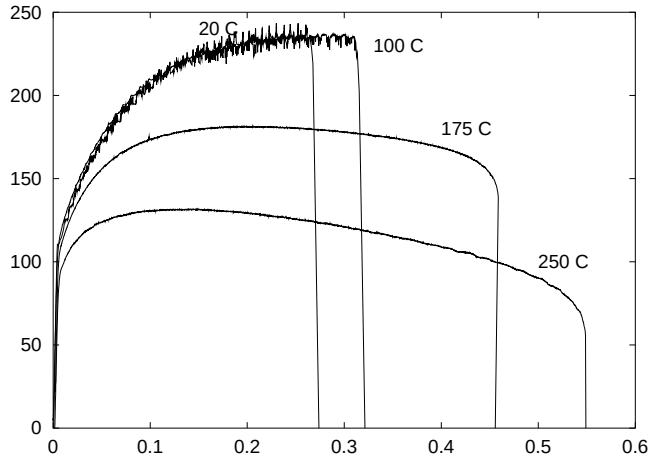


Figure 2: Measured engineering stress–strain curves at $\dot{\varepsilon} = 0.002$.

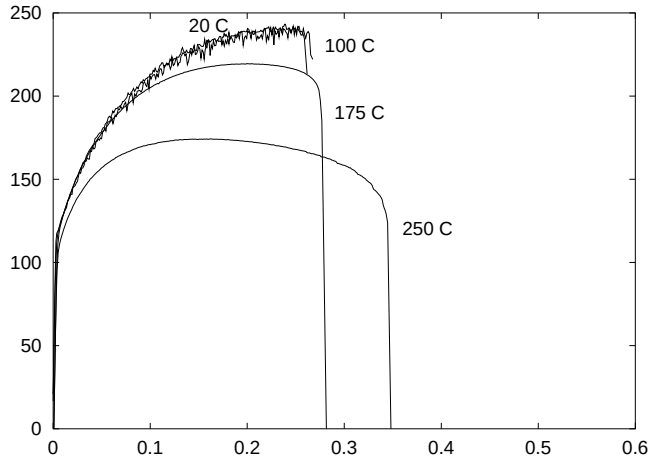


Figure 3: Measured engineering stress–strain curves at $\dot{\varepsilon} = 0.02$.

## 2.2 *The extended Nadai model*

The phenomenological model is based on the Nadai hardening law and power law strain rate dependency:

$$\sigma = C(\varepsilon + \varepsilon_0)^n \left(\frac{\dot{\varepsilon}}{\dot{\varepsilon}_0}\right)^m \tag{1}$$

The temperature dependence is included by letting $C$, $n$ and $m$ be functions of the temperature $T$ (in Kelvin). Starting of with simple exponential relations, we finally arrived at the following functions for the parameters, in order to fit the tensile tests.

$$C(T) = C_0 + a_1\left[1 - \exp\left(a_2\frac{T-273}{T_m}\right)\right] \tag{2a}$$

$$n(T) = n_0 + b_1\left[1 - \exp\left(b_2\frac{T-273}{T_m}\right)\right] \tag{2b}$$

$$m(T) = m_0 \exp\left(c\frac{T-273}{T_m}\right) \tag{2c}$$

The parameters were fitted to the uniaxial tensile tests as described in Section 2.1. The resulting values are presented in Table 1.

Table 1: Parameters for the extended Nadai model

| | | | |
|---|---|---|---|
| $T_m$ | 800 K | $n_0$ | 0.36 |
| $\varepsilon_0$ | 0.009 | $b_1$ | 0.07 |
| $C_0$ | 475 MPa | $b_2$ | 4 |
| $a_1$ | 110 | $m_0$ | 0.02 |
| $a_2$ | 4 | $c$ | 3 |
| $\dot{\varepsilon}_0$ | 0.0001 $s^{-1}$ | | |

## 2.3 *The Bergström model*

The physically based model used in this paper is a model described by Bergström and later adapted by Van Liempt (Bergström 1969; Bergström 1983; Van Liempt 1994). The model incorporates the influence of the temperature on the yield stress and on the hardening rate and includes recovery aspects. This model was initially used for the simulation of hot deformation of steel (Rietman 1999).

Basically the model determines the (equivalent) stress as:

$$\sigma = g(T)\left(\sigma_0 + \alpha G_{\text{ref}} b\sqrt{\rho} + \sigma^*(\dot{\varepsilon}, T)\right) \tag{3}$$

where the function $g(T)$ was originally defined by the ratio between the elastic shear modulus at temperature $T$ and at the reference temperature $T_{\text{ref}}$: $G(T)/G_{\text{ref}}$. The second part on the right-hand-side is the familiar Taylor equation see e.g. (Estrin 1996; Meyers 1999).

The essential part is the evolution of dislocation density $\rho$. This will give a temperature and strain rate influence on the hardening, while $\sigma^*$ yields an instantaneous temperature and strain rate influence on the flow stress. The dynamic stress $\sigma^*$ is commonly defined as

$$\sigma^*(\dot{\varepsilon}, T) = \sigma_0^*\left\{1 + \frac{kT}{\Delta G_0}\ln\left(\frac{\dot{\varepsilon}}{\dot{\varepsilon}_0}\right)\right\} \tag{4}$$

for $\dot{\varepsilon}_0 \exp(-\Delta G_0/kT) < \dot{\varepsilon} < \dot{\varepsilon}_0$ and with $k$ the Boltzmann number. From this equation, it can be seen that the influence of $\sigma^*$ decreases with increasing temperature. If Figures 2 and 3 are compared, it can be seen that there is hardly any influence of the strain rate on the initial yield stress and that the small influence that is present at low temperatures does not decrease at high temperatures. Therefore the contribution of $\sigma^*$ is neglected altogether in this paper. This means that all the influence of the temperature on the flow stress is introduced indirectly by the influence on the hardening rate. For fcc alloys, this behavior is also noted in the literature e.g. (Yao & Zajac 2000). Note that in the present extended Nadai model the strain-rate and temperature influence acts directly on the flow stress.

The evolution of dislocation density is formulated as a differential equation:

$$\frac{d\rho}{d\varepsilon} = U(\rho) - \Omega(\dot{\varepsilon}, T)\rho \tag{5a}$$

with

$$U = U_0\sqrt{\rho} \tag{5b}$$

$$\Omega = \Omega_0 + C\exp\left(-\frac{Q_v}{3RT}\right)\dot{\varepsilon}^{-\frac{1}{3}} \tag{5c}$$

The function $U$ represents storage of mobile dislocations (making them immobile) and $\Omega$ represents remobilization or dynamic recovery. The functions $U$, and especially the function $\Omega$ determine the shape of the hardening curve at different temperatures and strain rates.

The parameters were fitted to the uniaxial tensile tests as described in Section 2.1. The resulting values are presented in Table 2. The function $g(T)$ was fitted

Table 2: Parameters for the Bergström model

| | | | |
|---|---|---|---|
| $\sigma_0$ | 100 MPa | $\sigma^*$ | 0 MPa |
| $\alpha$ | 1.0 | $U_0$ | $5.5 \cdot 10^8\,\mathrm{m}^{-1}$ |
| $b$ | $2.857 \cdot 10^{-10}$ m | $\Omega_0$ | 17.5 |
| $C$ | 3070 | $Q_v$ | 87000 J/mole |

as a polynomial with the initial yield stress at a strain rate of 0.02 because the original scaling with $G(T)$ yielded a too strong decrease of the yield stress.

In Figures 4 and 5 the simulated engineering stress-strain curves are plotted, together with the experimental data. It can be seen that both models are more or less capable of describing the experiments. It should be noted that the comparison is only valid for uniform strain, so up to the maximum engineering stress.

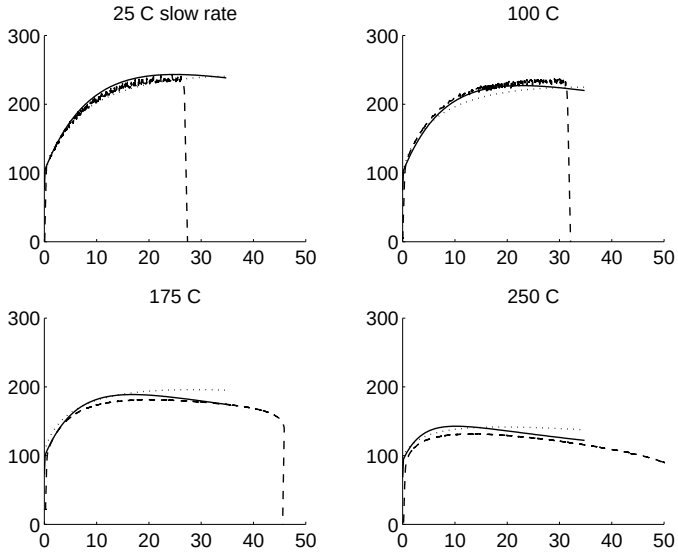


Figure 4: Stress–strain curves at different temperatures for $\dot{\varepsilon} = 0.002$, experiments (dashed), Bergström model (solid) and Nadai model (dotted).

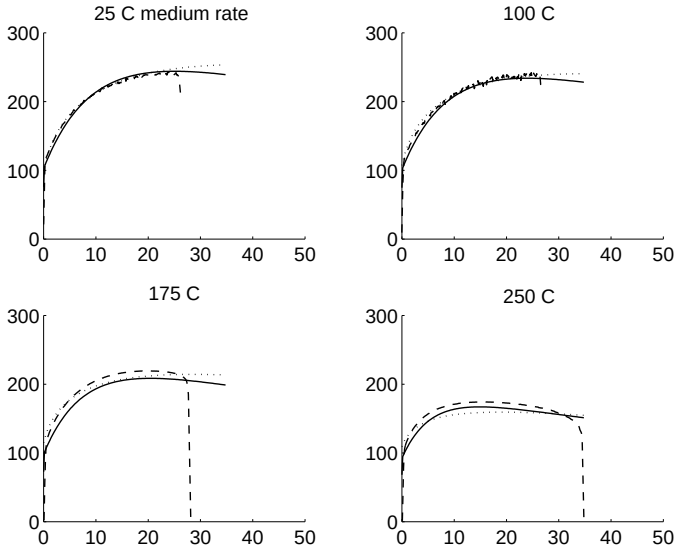


Figure 5: Stress–strain curves at different temperatures for $\dot{\varepsilon} = 0.02$, experiments (dashed), Bergström model (solid) and Nadai model (dotted).

## 3 EXPERIMENTS AND SIMULATIONS

A number of cylindrical cups have been deep drawn at different temperatures and with different punch velocities. These experiments have been simulated with the two material models, described in the previous section. Examples of test products are given in Figure 1.

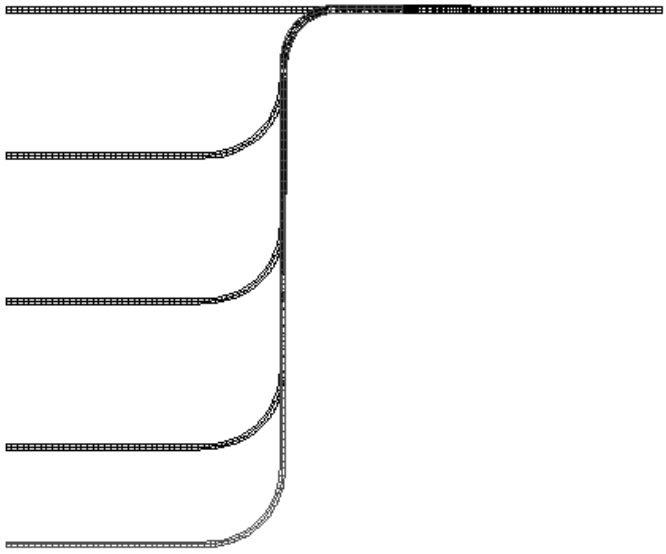

Figure 6: Element mesh at different punch displacements.

The simulation of the deep drawing experiments was performed with axi-symmetric elements. The sheets of 1.2 mm thickness were modeled with 2 elements in thickness direction and an element size of 1 mm in radial direction. The extended Nadai material model was implemented as a user routine in MSC.MARC. In this model also a part of the punch, die and blank holder were modeled, including heat rods and cooling channels. From these analyses, it appeared that the sheet in contact with the punch or the die/blank holder takes the temperature of that

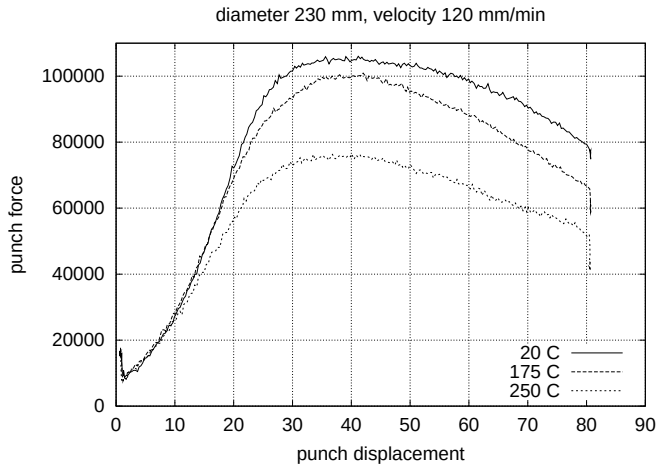


Figure 7: Experimental load-displacement curves for the punch at different temperatures.

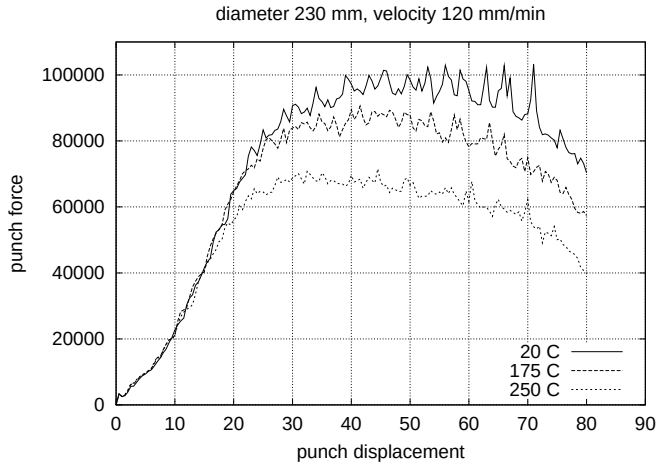


Figure 8: Punch load-displacement curves with the extended Nadai model at different temperatures.

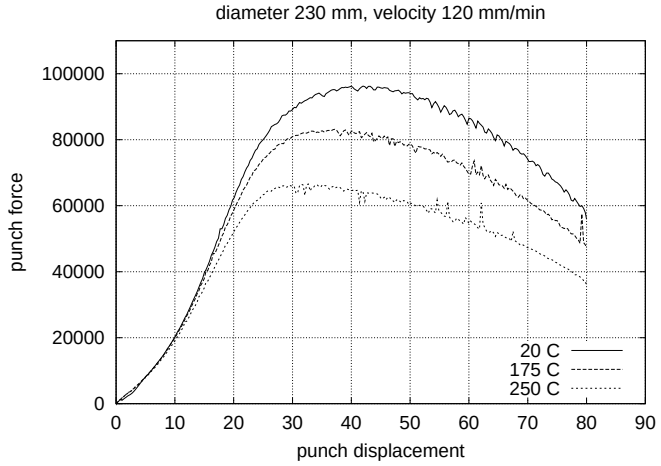


Figure 9: Punch load-displacement curves with the Bergström model at different temperatures.

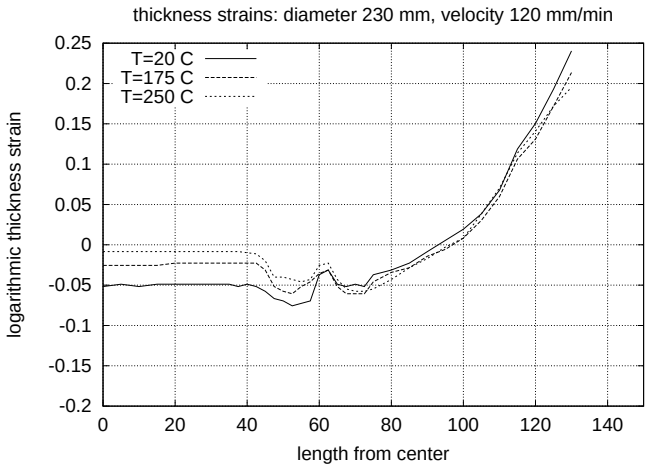


Figure 10: Experimental thickness distributions at different temperatures.

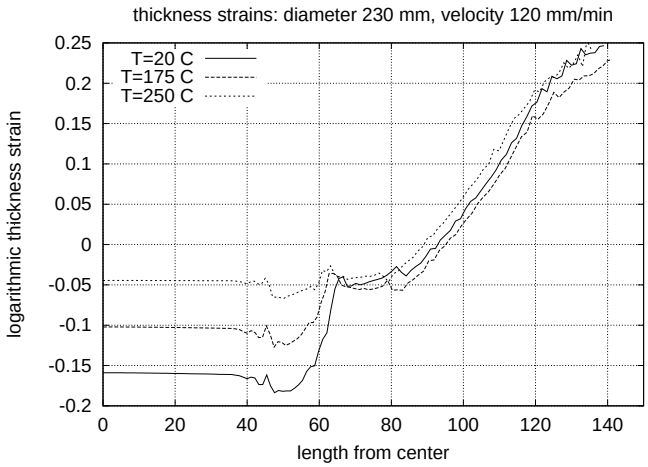


Figure 11: Thickness distribution with extended Nadai model at different temperatures.

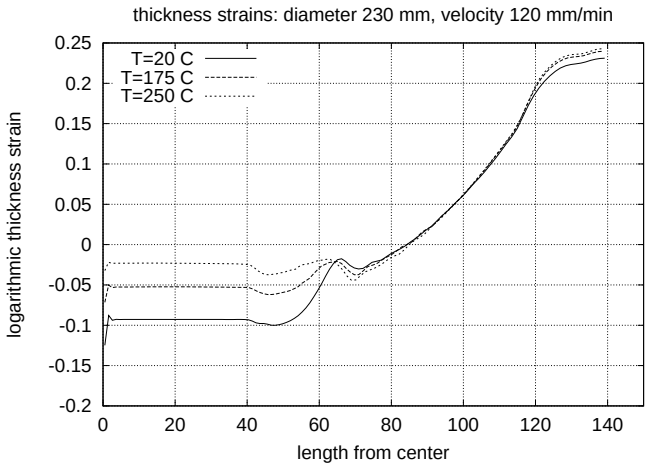


Figure 12: Thickness distributions with Bergström model at different temperatures.

tool, within some margin. The simulation with the Bergström model was performed with the in-house code DIEKA. Here the tools were modeled as rigid contours with a prescribed temperature. The undeformed and 4 deformed meshes of this simulation are presented in figure 6.

The friction between tool and workpiece is one of the least known factors in the simulations a Coulomb friction coefficient of 0.06 is assumed between tool and workpiece. This value was measured experimentally. It can be expected however that at high temperatures, the friction coefficient is higher than at low temperatures. All experiments and simulations were performed with blanks of 230 mm diameter and a punch stroke of 80 mm. The blank holder force was equivalent to an initial pressure of

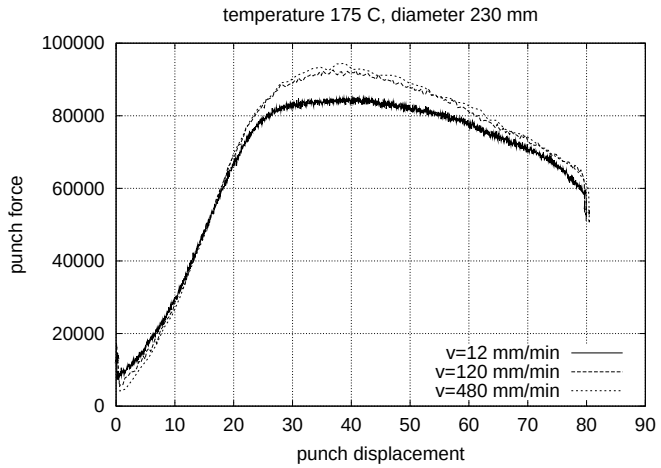


Figure 13: Experimental load-displacement curves for the punch at different punch velocities.

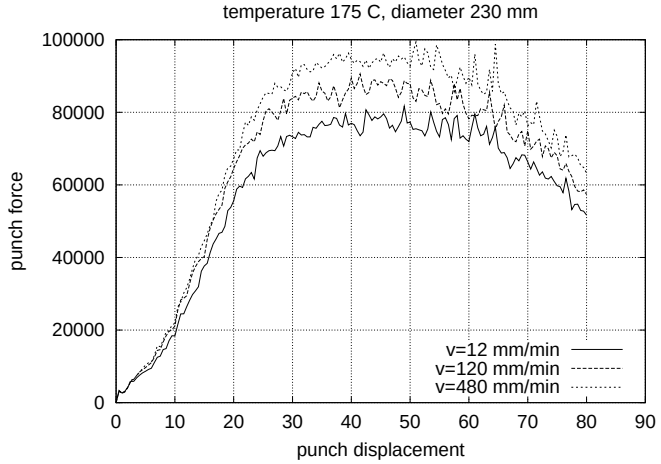


Figure 14: Punch load-displacement curves with the extended Nadai model at different punch velocities.

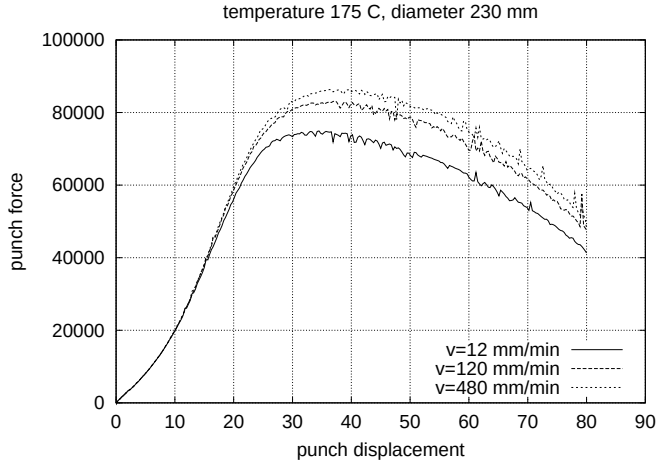


Figure 15: Punch load-displacement curves with the Bergström model at different punch velocities.

1.0 MPa. All mentioned temperatures are the temperatures of the die and blank holder. The punch is kept at 20 °C.

### 3.1 *Temperature influence*

Three experiments were performed with a punch velocity of 120 mm/min. The respective temperatures were 20°C, 175°C and 250°C. In Figures 7-9, the

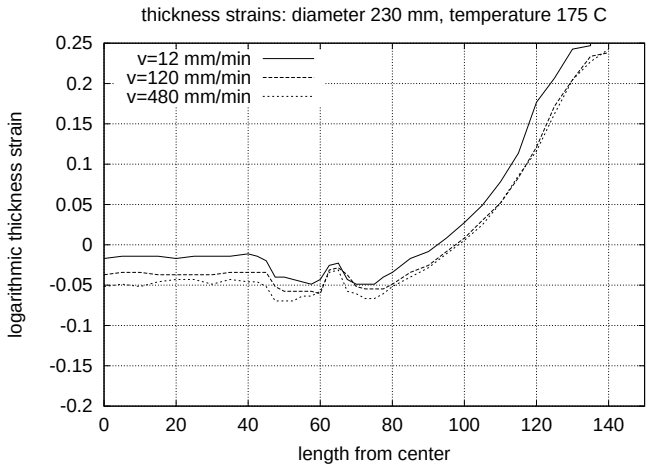


Figure 16: Experimental thickness distributions at different punch velocities.

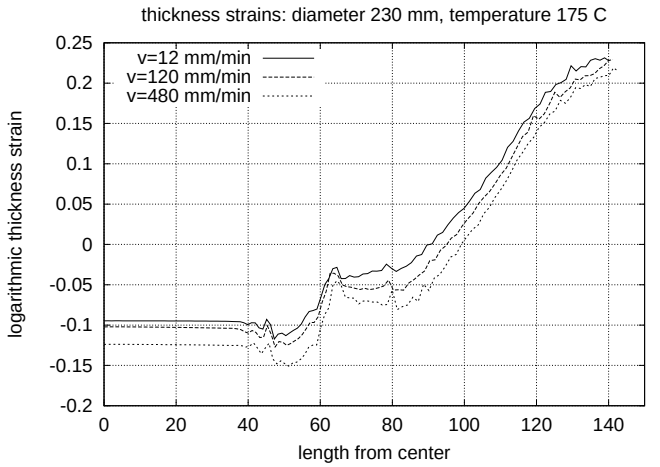


Figure 17: Thickness distribution with extended Nadai model at different punch velocities.

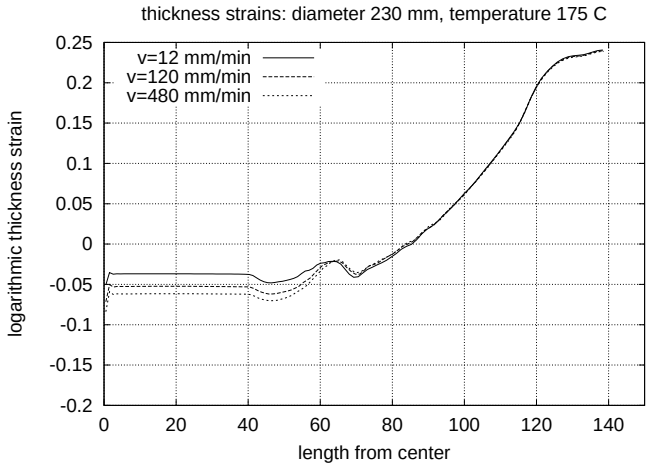


Figure 18: Thickness distributions with Bergström model at different punch velocities.

force-displacement diagrams of the punch are plotted for the experiments and the simulation with extended Nadai and Bergström model respectively.

In Figures 10-12, the thickness distributions of the cup at a depth of 80 mm are plotted for the experiments and the simulations.

### 3.2 *Punch velocity influence*

Three experiments were performed with a die temperature of 175°C and punch velocities of 12, 120 and 480 mm/min. In Figures 13-15 the experimental and simulated force-displacement curves for the punch are plotted.

In Figures 16-18 the experimental and simulated thickness distributions are plotted.

## 4 DISCUSSION

In the extended Nadai model the flow stress directly depends on the equivalent strain, strain-rate and temperature. In the Bergström model an evolution equation for the dislocation density is solved. As a result, the Nadai model will show a different flow stress upon strain rate change directly, while the Bergström model will reach a new flow stress only after some additional strain. It was expected that this difference would be clearly visible in the simulation of the deep drawing experiments, since there strain-rate and temperature are not constant.

Comparing the different punch force-displacement curves, it can be seen that both numerical models underestimate the experimental curves. The wiggles in the numerical curves are due to not fully converged increments. Since the extended Nadai model was used in an analysis model that included the thermal analysis of the die, blank holder and punch, the wiggles are more pronounced than with the Bergström model. This has nothing to do with the material models themselves.

The trends with changing temperature or punch velocity are predicted well, but the difference between 20 °C and 175 °C and between 120 mm/min and 480 mm/min are overestimated.

The change in thickness after 80 mm punch stroke is most pronounced in the bottom of the cup. Both numerical models predict this, but the extended Nadai model overestimates this considerably.

In the simulations of the deep drawing experiments the friction between tool and workpiece is one of the fundamental unknowns. Values, based on room temperature experience were used, but it is clear that these values are likely to change as the temperature increases. However high temperature experimental data are lacking. It is mainly attributed to the unknown friction conditions that the differences between simulation and experiment are rather large. Another reason may be the use of an isotropic Von Mises yield surface, while a non-isotropic and less smooth yield surface would be more appropriate. For the moment however, the actual shape of the yield surface at elevated temperatures can only be guessed.

With the deviations between simulation and experiment, the differences between the extended Nadai and the Bergström model can not be decisively interpreted as an advantage of one over the other.

## REFERENCES


Bergström, Y. (1969). Dislocation model for the stress-strain behaviour of polycrystalline α-Fe with special emphasis on the variation of the densities of mobile and immobile dislocations. *Mater. Sci. Eng. 5*, 193–200.

Bergström, Y. (1983). The plastic deformation of metals - a dislocation model and its applicability. *Reviews on Powder Metalurgy and Physical Ceramics 2*, 105–115.

Bolt, P., Lamboo, N. A. P. M., & Rozier, P. J. C. M. (1999). Feasibility of warm drawing of aluminium products. In M. Geiger, H. J. J. Kals, B. Shirvani, & U. P. Singh (Eds.), *Sheet Metal 1999*, Erlangen, pp. 575–580.

Bolt, P., Lamboo, N. A. P. M., Van Leeuwen, J. F. C., & Werkhoven, R. J. (2000). Warm drawing of aluminium components. In *Proceedings of the 7th Saxon Conference on Forming Technology, Lightweight Construction by Forming Technology*, Chemnitz, pp. 101–118.

Estrin, Y. (1996). Dislocation-density–related constitutive modeling. In A. S. Krausz & K. Krausz (Eds.), *Unified Constitutive Laws of Plastic Deformation*, pp. 69–104. San Diego: Academic Press.

Meyers, M. A. (1999). Dynamic deformation and failure. In M. A. Meyers, R. W. Armstrong, & H. O. K. Kirchner (Eds.), *Mechanics and Materials; Fundamentals and Linkages*, pp. 489–594. New York etc.: John Wiley & Sons, Inc.

Rietman, A. D. (1999). *Numerical Analysis of Inhomogeneous Deformation in Plane Strain Compression.* Ph. D. thesis, University of Twente.

Van Liempt, P. (1994). Workhardening and substructural geometry of metals. *J. Mater. Process. Technol. 45*, 459–464.

Wilson, D. V. (1988). Aluminium versus steel in the family car - the formability factor. *J. of Mech. Working Technol. 16*, 257–277.

Yao, X. & Zajac, S. (2000). The strain-rate dependence of flow stress and work-hardening rate in three Al-Mg alloys. *Scandinavian Journal of Metallurgy 29*, 101–107.